IEEE Access
Multidisciplinary | Rapid Review | Open Access Journal

Received 27 October 2023, accepted 15 December 2023, date of publication 25 December 2023,
date of current version 4 January 2024.

Digital Object Identifier 10.1109/ACCESS.2023.3346677

RESEARCH ARTICLE

A Stabilized Circuit-Consistent Foil Conductor Model

ELIAS PAAKKUNAINEN[1,2], JONAS BUNDSCHUH[1], IDOIA CORTES GARCIA[3], HERBERT DE GERSEM[1], (Member, IEEE), AND SEBASTIAN SCHÖPS[1], (Member, IEEE)

[1]Institute for Accelerator Science and Electromagnetic Fields, Technical University of Darmstadt, 64289 Darmstadt, Germany
[2]Electrical Engineering Unit, Tampere University, 33720 Tampere, Finland
[3]Department of Mechanical Engineering-Dynamics and Control, Eindhoven University of Technology, 5600 MB Eindhoven, The Netherlands

Corresponding author: Elias Paakkunainen (elias.paakkunainen@tu-darmstadt.de)

This work was supported by the German Science Foundation (DFG) under Grant 436819664. The work of Elias Paakkunainen and Jonas Bundschuh is supported by the Graduate School CE within Computational Engineering at the Technical University of Darmstadt.

ABSTRACT The magnetoquasistatic simulation of large power converters, in particular transformers, requires efficient models for their foils windings by means of homogenization techniques. Using the standard solid and stranded conductor models is not computationally feasible for a foil winding. In this article, the classical foil conductor model is derived and, for the first time, an inconsistency in terms of circuit theory is reported, which may lead to time-stepping instability. The inconsistency can be related to the differential-algebraic nature of the resulting system of equations. A new modified definition of the turn-by-turn conductance matrix of the foil conductor model is shown to mitigate this problem. The different structure of the systems using the alternative turn-by-turn conductance matrix definitions is examined in detail. Numerical results are presented to demonstrate the instability of the original foil conductor model and to verify the effectiveness of the new proposed model.

INDEX TERMS Foil conductor model, foil winding, differential algebraic equation, differential index, finite element method.

I. INTRODUCTION

Low-frequency electromagnetic field models are typically connected to a circuit model consisting of lumped elements to excite them [1]. This is done by means of conductor models that distribute circuit voltages and currents as electric fields and currents over the spatially resolved computational domain back and forth. The well-known terms solid and stranded conductor model have been coined in [2] and refined over the years, see e.g. [3] and [4] and the references therein.

In the design of e.g. transformers and magnetic components, foil windings are used [5], [6]. In comparison to litz windings, foil windings are easier to construct [7], and have better mechanical and thermal properties [6], [8]. However, for foil windings, the conventional conductor models become cumbersome because they require the individual thin sheets to be resolved on the computational domain. This leads to a very fine mesh and thus to a high, sometimes unmanageable number of degrees of freedom. As a remedy, foil conductor models [9], [10], [11] have been proposed. Figure 1 illustrates the foil winding geometry.

Sometimes field equations and conductor models are embedded into circuit simulations, for example if a power converter controller is simulated along with the device of interest [12]. The numerical treatment of such coupled problems has been investigated in [13], [14], [15], [16], and [17]. Two types of approaches can be distinguished: monolithic methods, where all equations are solved together in one large system, and co-simulation approaches, where the equations are solved separately with limited (possibly iterative) exchange of information. The numerical behavior of the resulting field/circuit coupled system has been analyzed in [18], [19], [20], and [21]. In conclusion: low-frequency magnetoquasistatic field models based on solid and stranded conductors shall be driven by voltages rather than currents to avoid numerical difficulties. This is consistent with their lumped equivalent model like (nonlinear) inductors, and it is independent of their potential formulation, i.e., $\vec{A}-\phi$ or $\vec{T}-\Omega$.

The associate editor coordinating the review of this manuscript and approving it for publication was Jenny Mahoney.

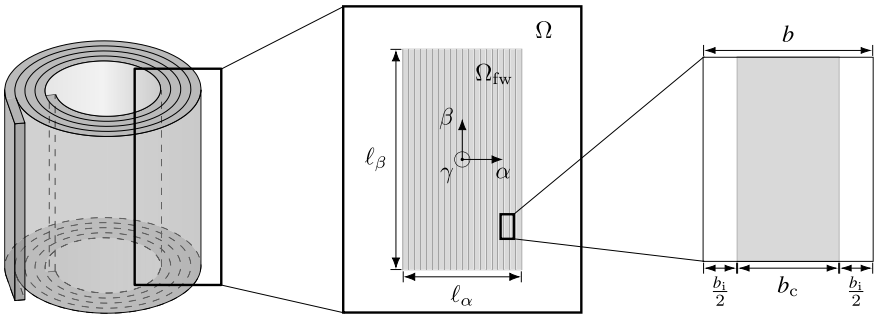

FIGURE 1. Illustration of the geometry of a foil winding. Left: A 3D sketch. Middle: Cross-section of the foil winding domain inside the computational domain with the local coordinate system (α, β, γ). Right: Cross-section of a single foil. The conducting material is colored in gray and the insulation material in white.

This paper extends the analysis of field/circuit coupled systems to the case of foil conductor models. We observe an issue with the conventional finite element (FE) approximation of the foil winding turn-by-turn conductance matrix and propose a new variant that restores the consistency with the inductance-like behavior of solid and stranded conductors.

The structure is as follows: Section II introduces the foil conductor model and describes its proposed modification. Section III examines how the model behaves as a part of an external circuit. In Section IV, numerical results are presented to verify the findings of the previous sections.

II. FOIL CONDUCTOR MODEL

Foil conductor models have been originally proposed in [9] and [10]. However, the following derivation follows mainly [11]. The model is derived for the three-dimensional setting as a natural generalization to special cases found in literature, for example the two-dimensional model in [9], and it coincides with the model of Dular and Geuzaine in [10]. Let us consider the magnetoquasistatic approximation of Maxwell's equations on a domain Ω, using the $\vec{A} - \phi$-formulation with the magnetic vector potential $\vec{A}$ and the electric scalar potential ϕ. Consequently, the electric field can be written as

$$\vec{E} = -\partial_t \vec{A} - \operatorname{grad} \phi \,. \tag{1}$$

We choose the scalar potential such that

$$-\operatorname{grad} \phi = \Phi \vec{\zeta} =: \vec{E}_\mathrm{s} \,, \tag{2}$$

with the voltage function Φ and a distribution function $\vec{\zeta}$ defined in the foil winding domain $\Omega_{\mathrm{fw}} := \operatorname{supp}(\vec{\zeta})$, where $\vec{\zeta}$ corresponds to the winding function for solid conductors from [22]. We assume that its direction is perpendicular to a constant rectangular cross-section

$$S = \left[-\frac{\ell_\alpha}{2}, \frac{\ell_\alpha}{2}\right] \times \left[-\frac{\ell_\beta}{2}, \frac{\ell_\beta}{2}\right], \tag{3}$$

see Fig. 1. To further simplify the notation, we introduce a local coordinate system $\alpha \in L_\alpha$, $\beta \in L_\beta$, $\gamma \in L_\gamma$ in the foil winding domain Ω_{fw} and use the (invertible) mapping $\mathbf{f} : (\alpha, \beta, \gamma) \mapsto (x, y, z)$ to transform local to global coordinates. We assume $\mathbf{f}$ to be linear in both α and β and to map the rectangle S to a rectangle in Ω. Note that not all of these assumptions are mathematically necessary but they cover all practical relevant cases. Finally, in the third dimension, the distribution function fulfills the property

$$\int_{\mathbf{f}(\alpha,\beta,L_\gamma)} \vec{\zeta} \cdot \mathrm{d}\vec{s} = 1 \,, \quad \forall \alpha \in L_\alpha \,, \ \forall \beta \in L_\beta \,. \tag{4}$$

Let us denote the number of turns with N. Then the domain of the k-th turn is described by $\Omega_k \subset \Omega_{\mathrm{fw}}$ such that $\Omega_{\mathrm{fw}} = \cup_{k=1}^{N} \Omega_k$. On each turn we define a restricted distribution function as

$$\vec{\zeta}_k = \begin{cases} \vec{\zeta} & \text{in } \Omega_k \,, \\ 0 & \text{else} \,. \end{cases} \tag{5}$$

The cross-section of a single foil (see the right side of Fig. 1), consists of a conducting material of width b_c and an insulation material of width b_i. The total width of one foil is b. The fill factor is defined $\lambda := \frac{b_\mathrm{c}}{b}$. We assume, due to insulation, that the electric field perpendicular to the foils, i.e., in α-direction of the local coordinate system, does not generate a current density.

To ensure that the total current flowing through every foil is equal to a lumped current i, it must hold

$$i = \int_\Omega \vec{J} \cdot \vec{\zeta}_k \, \mathrm{d}V \tag{6}$$

for all turns k, with $\vec{J}$ being the current density. We assume that the foils are thin with respect to the skin depth, i.e., $b_\mathrm{c} \ll \delta = \sqrt{\frac{2}{\omega\mu\sigma}}$, with the angular frequency ω, the permeability μ and the conductivity σ. With that, the current density can be assumed constant over the thickness of a foil. Since the conductivity in the insulation material σ_i is zero, the current density is only present in the conducting material. Consequently, (6) can be approximated using the conductivity of the conducting material σ_c with

$$i \approx b_\mathrm{c} \int_{\Gamma(\alpha_k)} \vec{J} \cdot \vec{\zeta} \, \mathrm{d}S = b_\mathrm{c} \int_{\Gamma(\alpha_k)} \sigma_\mathrm{c} \vec{E} \cdot \vec{\zeta} \, \mathrm{d}S \,. \tag{7}$$

Herein, $\Gamma(\alpha)$ is the surface through the foil winding domain at position α, i.e.

$$\Gamma(\alpha) := \left\{ \mathbf{f}(\alpha, \beta, \gamma) : \beta \in L_\beta, \ \gamma \in L_\gamma \right\} \subset \Omega_{\mathrm{fw}} \,, \tag{8}$$

and α_k is the midpoint coordinate of the k-th turn. Lastly, we insert the expression for $\vec{E}$ and write

$$i \approx b \int_{\Gamma(\alpha_k)} \lambda \sigma_\mathrm{c} \left(-\partial_t \vec{A} + \Phi \vec{\zeta} \right) \cdot \vec{\zeta} \, \mathrm{d}S \,. \tag{9}$$

In the homogenized model, the single foils are not resolved anymore. The foil winding domain has constant anisotropic material parameters of a homogenized conductivity and reluctivity that are determined with a mixing rule [23]. Therefore, in the foil winding domain, we write

$$\sigma_\alpha = 0 \,, \tag{10a}$$
$$\sigma_\beta = \sigma_\gamma = \lambda \sigma_\mathrm{c} + (1-\lambda)\sigma_\mathrm{i} = \lambda \sigma_\mathrm{c} \,, \tag{10b}$$
$$\nu_\alpha = \lambda \nu_\mathrm{c} + (1-\lambda)\nu_\mathrm{i} \,, \tag{10c}$$
$$\nu_\beta = \nu_\gamma = \left(\frac{\lambda}{\nu_\mathrm{c}} + \frac{(1-\lambda)}{\nu_\mathrm{i}} \right)^{-1} \,. \tag{10d}$$

The current condition (9) has to hold for all α_k. For $N \to \infty$, we impose (9) for all $\alpha \in L_\alpha$. We end up with the final, homogenized system of equations

$$\operatorname{curl}\left(\nu \operatorname{curl} \vec{A} \right) + \sigma \partial_t \vec{A} - \sigma \Phi \vec{\zeta} = 0 \,, \quad \text{in } \Omega \tag{11a}$$
$$\int_{\Gamma(\alpha)} \sigma \left(-\partial_t \vec{A} + \Phi \vec{\zeta} \right) \cdot \vec{\zeta} \, \mathrm{d}S = \frac{i}{b} \,, \quad \text{in } L_\alpha \tag{11b}$$

with adequate initial values and boundary conditions on $\partial\Omega$. We choose, for simplicity of notation, a homogenous Dirichlet condition, i.e., $\vec{A} \times \vec{n} = 0$ on $\partial\Omega$ where $\vec{n}$ is the outward pointing normal vector.

A. DISCRETIZED MODEL

In the following, (11) is discretized using the Galerkin procedure [24], [25]. The vector potential $\vec{A}$ is discretized with a finite set of standard FE edge functions $\vec{w}_j \in \mathbf{H}_0(\mathrm{curl}, \Omega)$. We assume that the distribution function $\vec{\zeta}$ can be expressed in terms of the same $\vec{w}_j$ or is approximated by L2 projection. Finally, the voltage function Φ is discretized with another set of basis functions $\hat{p}_l \in H^1(L_\alpha)$ which are defined in the local coordinate system but can be transformed with

$$p_l(x,y,z) = \begin{cases} \hat{p}_l \circ f_\alpha^{-1}(x,y,z) & \text{if } (x,y,z) \in \Omega_\mathrm{fw} \,, \\ 0 & \text{otherwise} \,, \end{cases} \tag{12}$$

where $f_\alpha^{-1}(x,y,z)$ denotes the α-component of the inverse of $\mathbf{f}$. This allows us to expand the fields in terms of the basis functions defined on Ω as

$$\vec{A} = \sum_{j=1}^{N_w} a_j \vec{w}_j, \quad \vec{\zeta} = \sum_{j=1}^{N_w} x_j \vec{w}_j \quad \text{and} \quad \Phi = \sum_{l=1}^{N_p} u_l p_l \,, \tag{13}$$

where we do not distinguish between the exact fields and their FE approximations. The unknown coefficients of the system are $[\mathbf{a}]_i = a_i$ and $[\mathbf{u}]_i = u_i$. The discretization of $\vec{\zeta}$ does not introduce additional unknowns as it is determined beforehand, e.g., by solving a stationary current flow problem, see [22] and [26].

Testing (11a) with edge functions $\vec{w}_i$ and integration over the computational domain Ω yield the standard FE matrices $\mathbf{K}_\nu, \mathbf{M}_\sigma \in \mathbb{R}^{N_w \times N_w}$ and the vector $\mathbf{X}_\sigma \in \mathbb{R}^{N_w \times N_p}$. Their entries are

$$[\mathbf{K}_\nu]_{i,j} = \int_\Omega \nu \operatorname{curl} \vec{w}_j \cdot \operatorname{curl} \vec{w}_i \, \mathrm{d}V \,, \tag{14}$$
$$[\mathbf{M}_\sigma]_{i,j} = \int_\Omega \sigma \vec{w}_j \cdot \vec{w}_i \, \mathrm{d}V \,, \tag{15}$$
$$[\mathbf{X}_\sigma]_{i,l} = \int_\Omega \sigma p_l \vec{\zeta} \cdot \vec{w}_i \, \mathrm{d}V \,. \tag{16}$$

Following the naming convention from mechanics, we call $\mathbf{K}_\nu$ the stiffness matrix and $\mathbf{M}_\sigma$ the mass matrix. Since the distribution function $\vec{\zeta}$ can be expressed in terms of the FE edge functions $\vec{w}_j$, see (13), it holds

$$[\mathbf{X}_\sigma]_{i,l} = \sum_j x_j \int_\Omega \sigma p_l \vec{w}_j \cdot \vec{w}_i \, \mathrm{d}V \tag{17}$$
$$= \left[\mathbf{M}_{\sigma,l} \mathbf{x} \right]_i \,, \tag{18}$$

with $[\mathbf{x}]_i = x_i$ being the coefficients of the distribution function and $[\mathbf{M}_{\sigma,l}]_{i,j} = \int_\Omega \sigma p_l \vec{w}_j \cdot \vec{w}_i \, \mathrm{d}V$ the (modified) mass matrix containing the extra basis functions.

The current condition (11b) is tested with the basis functions p_k and integrated over the one-dimensional domain $\mathbf{f}(L_\alpha, \beta, \gamma)$ of homogenization, i.e.

$$\int_\Omega \sigma \left(-\partial_t \vec{A} + \Phi \vec{\zeta} \right) \cdot \vec{\zeta} p_k \, \mathrm{d}V = \int_{\mathbf{f}(L_\alpha,\beta,\gamma)} \frac{i}{b} p_k \, \mathrm{d}s \,. \tag{19}$$

This yields the transpose of the already defined matrix $\mathbf{X}_\sigma$, the vector $\mathbf{c} \in \mathbb{R}^{N_p}$ and the turn-by-turn conductance matrix $\mathbf{G} \in \mathbb{R}^{N_p \times N_p}$, whose entries are defined as

$$[\mathbf{c}]_k = \frac{1}{b} \int_{\mathbf{f}(L_\alpha,\beta,\gamma)} p_k \, \mathrm{d}s = \frac{N}{\ell_\alpha} \int_{\mathbf{f}(L_\alpha,\beta,\gamma)} p_k \, \mathrm{d}s \,, \tag{20}$$

and

$$[\mathbf{G}]_{k,l} = \int_\Omega \sigma \vec{\zeta} \cdot \vec{\zeta} p_l p_k \, \mathrm{d}V \tag{21}$$
$$= \sum_{i,j=1}^{N_w} x_i x_j \int_\Omega \sigma \vec{w}_i \cdot \vec{w}_j p_l p_k \, \mathrm{d}V \tag{22}$$
$$= \mathbf{x}^\top \mathbf{M}_{\sigma,k,l} \mathbf{x} \,. \tag{23}$$

The turn-by-turn conductance matrix can be expressed using the (modified) mass matrices $\left[\mathbf{M}_{\sigma,k,l}\right] = \int_\Omega \sigma \vec{w}_i \cdot \vec{w}_j p_l p_k \, \mathrm{d}V$ involving both p_k and p_l.

The voltage drop v over the foil winding domain is the sum of the voltage drops over each foil, i.e.

$$v = \sum_{k=1}^{N} v_k \,. \tag{24}$$

With the voltage function, we can approximate the voltage drop over foil k as $v_k = \Phi(\mathbf{f}(\alpha_k, \cdot, \cdot))$. From there, it follows

$$v = \sum_k \Phi(\mathbf{f}(\alpha_k, \cdot, \cdot)) \approx \sum_k \frac{1}{\delta} \int_{\alpha_k - \frac{\delta}{2}}^{\alpha_k + \frac{\delta}{2}} \Phi(\mathbf{f}(\alpha, \cdot, \cdot)) \, \mathrm{d}\alpha \tag{25}$$

$$= \frac{1}{\delta} \int_{L_\alpha} \Phi(\mathbf{f}(\alpha, \cdot, \cdot))\, \mathrm{d}\alpha \tag{26}$$

$$= \frac{1}{b} \int_{\mathbf{f}(L_\alpha, \beta, \gamma)} \Phi\, \mathrm{d}s. \tag{27}$$

Consequently, the voltage can be expressed with $v = \mathbf{c}^\top \mathbf{u}$. Finally, the discretized foil conductor model can be expressed in terms of the matrices above as

$$\mathbf{M}_\sigma \frac{\mathrm{d}}{\mathrm{d}t}\mathbf{a} + \mathbf{K}_\nu \mathbf{a} - \mathbf{X}_\sigma \mathbf{u} = \mathbf{0} \tag{28a}$$

$$-\mathbf{X}_\sigma^\top \frac{\mathrm{d}}{\mathrm{d}t}\mathbf{a} + \mathbf{G}\mathbf{u} - \mathbf{c}i = \mathbf{0} \tag{28b}$$

$$-\mathbf{c}^\top \mathbf{u} + v = 0 \tag{28c}$$

with appropriate initial values at some time t_0.

B. ALTERNATIVE DISCRETIZATION OF THE TURN-BY-TURN CONDUCTANCE MATRIX

We propose an alternative discretization of the turn-by-turn conductance matrix (21). We start by introducing the source electric field corresponding to voltage v_l as an explicit variable

$$\vec{E}_{\mathrm{s},l} = p_l \vec{\zeta} = \sum_{j=1}^{N_w} e_{l,j} \vec{w}_j \tag{29}$$

and use this in (21) such that

$$[\mathbf{G}_e]_{k,l} = \int_\Omega \sigma p_k \vec{\zeta} \cdot \vec{E}_{\mathrm{s},l}\, \mathrm{d}V \tag{30}$$

$$= \sum_{i,j} x_i e_{l,j} \int_\Omega \sigma p_k \vec{w}_i \cdot \vec{w}_j\, \mathrm{d}V \tag{31}$$

$$= \mathbf{x}^\top \mathbf{M}_{\sigma,k} \mathbf{e}_l \tag{32}$$

and for all $j = 1, \ldots, N_w$

$$\int_\Omega \sigma \vec{w}_j \cdot \vec{E}_{\mathrm{s},l}\, \mathrm{d}V = \int_\Omega \sigma \vec{w}_j \cdot \left(p_l \vec{\zeta}\right)\, \mathrm{d}V \tag{33}$$

$$\sum_i e_{l,i} \int_\Omega \sigma \vec{w}_j \cdot \vec{w}_i\, \mathrm{d}V = \sum_i x_i \int_\Omega \sigma p_l \vec{w}_j \cdot \vec{w}_i\, \mathrm{d}V \tag{34}$$

$$\mathbf{M}_\sigma \mathbf{e}_l = \mathbf{M}_{\sigma,l} \mathbf{x}\,. \tag{35}$$

Plugging $\mathbf{e}_l$ into the above equation yields another variant of the turn-by-turn conductance matrix, i.e.,

$$[\mathbf{G}_e]_{k,l} = \mathbf{x}^\top \mathbf{M}_{\sigma,k} \mathbf{M}_\sigma^+ \mathbf{M}_{\sigma,l} \mathbf{x}\,, \tag{36}$$

where $\mathbf{M}_\sigma^+$ denotes the (Moore-Penrose) pseudo-inverse of $\mathbf{M}_\sigma$. This mass matrix is singular because it only acts on degrees of freedom that are located in conductive domains. However, this is sufficient since the source electric fields are located exactly there.

Note that both definitions, i.e., (21) and (36), lead in general to different matrices for finitely many basis functions. However, for a given voltage discretization with polynomial degree N_p, both converge to the same solution for $N_w \to \infty$ as will be demonstrated in the numerical example in Section IV.

C. COMPATIBILITY WITH SOLID CONDUCTOR MODEL

In [11], it is stated that the foil conductor model behaves as a solid conductor if a constant voltage function is chosen, i.e., $p_1 = 1$ is the only basis function ($N_p = 1$). In this special case the definitions (14) and (15) do not change but (18) naturally simplifies to

$$\mathbf{x}_{\mathrm{sol}} = \mathbf{M}_\sigma \mathbf{x}\,. \tag{37}$$

Both the original (21) and the new discretization (36) of the turn-by-turn conductance matrix reduce to

$$G_{\mathrm{sol}} = \mathbf{x}^\top \mathbf{M}_\sigma \mathbf{x} \tag{38}$$

$$= \mathbf{x}^\top \mathbf{M}_\sigma \mathbf{M}_\sigma^+ \mathbf{M}_\sigma \mathbf{x}\,. \tag{39}$$

From this, it follows that the foil conductor model is equivalent to the classic solid conductor model [22] for both variants of the conductance matrices. It reads

$$\mathbf{M}_\sigma \frac{\mathrm{d}}{\mathrm{d}t}\mathbf{a} + \mathbf{K}_\nu \mathbf{a} - \mathbf{x}_{\mathrm{sol}} v = \mathbf{0} \tag{40a}$$

$$-\mathbf{x}_{\mathrm{sol}}^\top \frac{\mathrm{d}}{\mathrm{d}t}\mathbf{a} + G_{\mathrm{sol}} v - i = 0\,. \tag{40b}$$

since the third equation (28c) becomes trivial, i.e., $u_1 = v$, and can be plugged into the second (28b).

III. CIRCUIT COMPATIBILITY

The conductor models, i.e., foil (28) and solid (40), provide the necessary coupling conditions for circuits, i.e., they allow to excite the electromagnetic fields in terms of currents and voltages. Since the mid 70s, the most common formalism implemented in circuit simulators is the modified nodal analysis (MNA) [27]. Its main advantages are sparse system matrices that are easy to assemble and its robustness with respect to topological changes, e.g., switching. While the MNA is formulated in less unknowns than for example sparse tableau analysis [28], it does not aim for a minimal set of degrees of freedom. One consequence of this redundancy is that the resulting system consists of differential and algebraic equations (DAEs) rather than ordinary differential equations (ODEs). Common issues related to the numerical treatment of DAEs are the difficulty of finding consistent initial conditions and the sensitivity towards perturbations [29].

A. SENSITIVITY WITH RESPECT TO PERTURBATIONS

To illustrate these numerical difficulties, we consider a simple inductor model in flux-oriented form, i.e.,

$$\frac{\mathrm{d}}{\mathrm{d}t}\psi(t) = v(t) \tag{41a}$$

$$\psi(t) = Li(t) \tag{41b}$$

for $t \in (t_0, t_{\mathrm{end}}]$. The equations describe a relation between currents and voltages. Let us investigate the voltage- and current-driven-case separately, see Fig. 2.

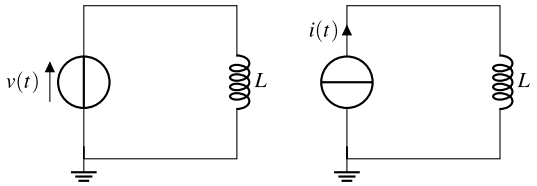

FIGURE 2. Voltage- (left) and current-driven (right) inductor.

1) VOLTAGE-DRIVEN CASE

For a given voltage v the problem is described in terms of a differential equation defining the flux ψ and an algebraic equation for the current i. After time-differentiation of (41b) one obtains a purely differential problem. The solution is

$$i(t) = \frac{1}{L}\left(\psi_0 + \int_{t_0}^{t} v(s)\mathrm{d}s\right) \tag{42}$$

with an arbitrary flux $\psi(t_0) = \psi_0$ as initial condition.

2) CURRENT-DRIVEN CASE

If the current i is given, then ψ is fixed by an algebraic relation and the solution is

$$v(t) = L\frac{\mathrm{d}}{\mathrm{d}t}i(t). \tag{43}$$

This is an algebraic equation that does not allow to freely specify an initial condition or more precisely: only $v(t_0) = v_0 := L\frac{\mathrm{d}}{\mathrm{d}t}i(t)|_{t_0}$ is consistent. Note that this equation is obtained with one time-differentiation of (41b). Only after a second differentiation an explicit ODE for $\frac{\mathrm{d}}{\mathrm{d}t}v$ can be obtained.

B. DIFFERENTIAL INDEX

The sensitivity of the solution with respect to perturbations is very different in the systems of Section III-A1 and III-A2. Let us consider the following particular current excitation for the current-driven case

$$i(t) = I_1 \sin(2\pi f_1 t) + I_2 \sin(2\pi f_2 t) \tag{44}$$

where the second amplitude shall be almost negligible $I_2 \ll I_1$ but at very high frequency $f_2 \gg I_1/I_2 f_1$. Due to the time-derivative in (43) the solution in the current-driven case will be seriously perturbed, i.e., the second term with amplitude $2\pi f_2 I_2$ becomes dominant. On the other hand, a similarly perturbed voltage source would not significantly affect the current of the voltage-driven case (42) since there, in the solution, the sum of the sine waves appears integrated in time instead of differentiated.

This motivates the introduction of the number of time-differentiations as a measure of sensitivity and classification of DAEs. In this context, the notion of index of a DAE is proposed. Several definitions exist. We use the following:

Definition 1. *(Differential index [30]) A solvable and sufficiently smooth system of DAEs* $\mathbf{f}(\mathbf{x}', \mathbf{x}, t) = \mathbf{0}$ *is said to have differential index m, if m is the minimum number of differentiations*

$$\frac{\mathrm{d}}{\mathrm{d}t}\mathbf{f}(\mathbf{x}', \mathbf{x}, t) = \mathbf{0}, \quad \ldots, \quad \frac{\mathrm{d}^m}{\mathrm{d}t^m}\mathbf{f}(\mathbf{x}', \mathbf{x}, t) = \mathbf{0},$$

that allow the extraction of an explicit ordinary differential system with only algebraic manipulations.

For circuits modeled with MNA containing classical lumped circuit elements, the differential index is known and depends on the topology of the circuit [31]. The index is 2 at maximum. The following theorem states the condition for this case, however, without formulating all necessary assumptions for which the reader is referred to the original paper.

Theorem 1. *(Differential index of circuits [31]) Circuits modeled with MNA lead to systems of DAEs with differential index 2 if, and only if, at least one of the following conditions is fulfilled. The circuit contains*

(i) cutsets of branches which contain only inductors and current sources. ("LI-cutsets").

(ii) loops of branches which contain only capacitors and voltage sources ("CV-loops") with at least one voltage source.

Otherwise, the circuit has differential index 1.

The theorem is immediately applicable to our two simple inductor examples. The first case, Section III-A1, is a series connection of an inductor and a voltage source which is at most index 1 and harmless. The second example, Section III-A2, forms a *LI*-cutset and may lead to numerical problems, e.g., high sensitivity towards noise as observed.

C. CLASSIFICATIONS

Generalized circuit elements have been introduced in [32] to classify field models as refined elements and to include them in the index result of Theorem 1. Resistance-like, inductance-like and capacitance-like elements are defined. Classical resistances, capacitors and inductors, as well as charge formulated capacitances and flux formulated inductances have been shown to correspond to their generalized circuit elements. The type of generalized element, that the field model is, gives an intuition how the model will behave in an external circuit. Given the intuitively inductive nature of the foil conductor model, we focus on the introduction of the inductance-like element. The resistance-like element is briefly remarked.

In the following, a simplified version of the (strongly) inductance-like element definition [32] will be used. The definition is more restrictive but still sufficient for the analysis of linear systems such as the foil conductor model discussed here.

Definition 2. *(Inductance-like element) A circuit element is called inductance-like, if with only one time differentiation its constitutive equations can be transformed into the form*

$$\frac{\mathrm{d}}{\mathrm{d}t}\mathbf{x} = \mathbf{f}_{\mathbf{x}}(\mathbf{x}, i, v, t) \tag{45a}$$

$$\frac{\mathrm{d}}{\mathrm{d}t}i = g_{\mathrm{L}}(\mathbf{x}, i, v, t) \tag{45b}$$

where $\mathbf{x}$ *are 'internal' variables that are not explicitly coupled to the circuit (e.g., vector potentials). Additionally,*

$$\partial_v g_{\mathrm{L}}(\mathbf{x}, i, v, t) := L \tag{46}$$

is required to be positive (definite).

In addition to inductance-like, [32] defines resistance-like and capacitance-like elements. Roughly speaking, a (simplified) resistance-like element is defined similarly to the inductance-like element in Definition 2, with the key difference being that the implicit relation between the current i and the voltage v is

$$\frac{\mathrm{d}}{\mathrm{d}t}i = g_{\mathrm{R}}(\frac{\mathrm{d}}{\mathrm{d}t}v, \mathbf{x}, i, v, t), \tag{47}$$

where $\partial_{v'} g_{\mathrm{R}}(v', \mathbf{x}, i, v, t) := G_{\mathrm{R}}$ is positive (definite). For a formal definition of resistance-like as well as capacitance-like elements we refer to [32].

The conclusions drawn in Section III-B for the differential index of the circuits containing only an inductance and a source as well as Theorem 1 remain unchanged if the elements are replaced with their generalized definitions.

D. INDUCTANCE-LIKE BEHAVIOR

In this section, the previously introduced mathematical concepts are utilized to analyze the foil conductor model which uses the proposed turn-by-turn conductance matrix (36). We seek to prove that the model is an inductance-like element.

Assumption 1. *Gauged field formulation with consistent excitation*

(i) $\mathbf{X}_\sigma$ *has full column rank.*

(ii) The field formulation is adequately gauged such that the matrix pencil $\tau\mathbf{M}_\sigma + \mathbf{K}_\nu$ *is regular, i.e.,* $\det(\tau\mathbf{M}_\sigma + \mathbf{K}_\nu) \neq 0$ *for* $\tau \in \mathbb{R}$.

Property (i) describes a consistent excitation. The condition for (ii) is automatically fulfilled when the calculation is done in 2D. In 3D, an additional gauging condition needs to be imposed, such as, e.g., a tree-cotree gauge [33].

Using Property (i) of Assumption 1 leads to $\mathbf{G}_e$ being invertible. Consequently, the system of equations (28) can be written as

$$\underbrace{\left(\mathbf{M}_\sigma - \mathbf{X}_\sigma \mathbf{G}_e^{-1} \mathbf{X}_\sigma^\top\right)}_{:=\bar{\mathbf{M}}} \frac{\mathrm{d}}{\mathrm{d}t}\mathbf{a} + \mathbf{K}_\nu \mathbf{a} = \underbrace{\mathbf{X}_\sigma \mathbf{G}_e^{-1}\mathbf{c}}_{:=\bar{\mathbf{x}}} i \tag{48a}$$

$$\underbrace{\mathbf{c}^\top \mathbf{G}_e^{-1} \mathbf{X}_\sigma^\top}_{=\bar{\mathbf{x}}^\top} \frac{\mathrm{d}}{\mathrm{d}t}\mathbf{a} + \underbrace{\mathbf{c}^\top \mathbf{G}_e^{-1}\mathbf{c}}_{:=R} i = v \tag{48b}$$

by solving (28b) with respect to $\mathbf{u}$, and substituting it in (28a) and (28c). Note that (48) has the same structure as the stranded conductor model, which is known to be an inductance-like element [20].

Proposition 1. *The foil conductor model according to (48) using the proposed turn-by-turn conductance matrix (36) is an inductance-like element.*

Proof. The proof is presented in Appendix I. □

Note that $\mathbf{u}$ is part of the internal variables of the inductance-like element in the foil conductor model and is not explicitly coupled to the circuit. Therefore, its behavior will not influence the circuit itself, and it can be left out of the proof. Examinations suggest that it is an index-2 variable. This, however, does not influence the index of the circuit's variables.

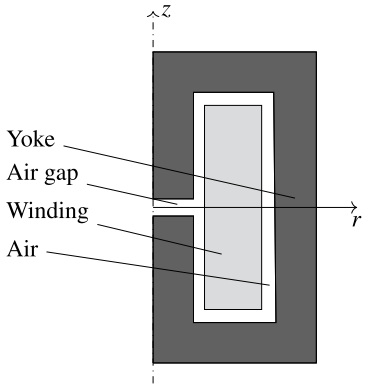

FIGURE 3. Simulation domain for the numerical tests.

E. (SINGULARLY PERTURBED) RESISTANCE-LIKE BEHAVIOR

Similarly to the analysis for (48), the original system (28) with the original turn-by-turn conductance matrix $\mathbf{G}$ as defined in (21) can be classified according to the generalized circuit elements of [32].

Proposition 2. *The foil conductor model (28) with the original turn-by-turn conductance matrix (21) is a resistance-like element.*

Proof. The proof is given in Appendix II. □

The key difference between both cases is that, whereas in our redefined conductance we replace $\mathbf{G}$ with $\mathbf{G}_e$ and, therefore, $\frac{\partial g_{\mathrm{R}}}{\partial v'} = (\mathbf{c}^\top(\mathbf{G} - \mathbf{G}_e)^{-1}\mathbf{c})^{-1} = 0$ (see Appendix II), in the original conductance computation, $\mathbf{G} \neq \mathbf{G}_e$. Intuitively, this inconsistency arises as $\mathbf{G}$ corresponds to the natural discretization of the foil conductor's conductance but only $\mathbf{G}_e$ is consistent with the discrete spaces spanned by the finite element matrices.

Remark. We say the foil conductor model (28) with the original turn-by-turn conductance matrix (21) is singularly perturbed resistance-like, as its resistance-like behavior depends on the positive definiteness of $\frac{\partial g_{\mathrm{R}}}{\partial v'} = (\mathbf{c}^\top(\mathbf{G} - \mathbf{G}_e)^{-1}\mathbf{c})^{-1}$. This expression imposes the (linear) relation between $\frac{\mathrm{d}}{\mathrm{d}t}i$ and $\frac{\mathrm{d}}{\mathrm{d}t}v$ in (47). Thus, if the term is positive definite, the element is resistance-like. However, when refining the finite element discretization $N_w \to \infty$ for a given voltage discretization with polynomial degree N_p, that term tends to zero, and the model degenerates into an inductance-like element.

IV. NUMERICAL RESULTS

A numerical implementation of the foil conductor model according to (28) is done for both of the turn-by-turn conductance matrix definitions (21) and (36) using the FE simulation framework *Pyrit* [34]. The considered modeling domain is shown in Fig. 3. Table 1 contains the simulation specifications and the values used for the material parameters.

TABLE 1. Simulation specifications and material parameters.

Quantity	Symbol	Value
Number of voltage basis functions	N_p	5
Number of foils	N	50
Fill factor	λ	0.8
Foil thickness	b	0.28 mm
Foil height	ℓ_β	50 mm
Air gap length	-	4.2 mm
Yoke height	-	76.2 mm
Yoke outer radius	-	40 mm
Frequency	f	50 Hz
Perturbation frequency	f_ϵ	$2\pi \cdot 10^{10}$ Hz
Perturbation amplitude	ϵ	10^{-3}
Foil winding conductivity	σ	$6 \cdot 10^7$ S m^{-1}
Yoke conductivity	-	10 S m^{-1}
Yoke relative permeability	-	1000

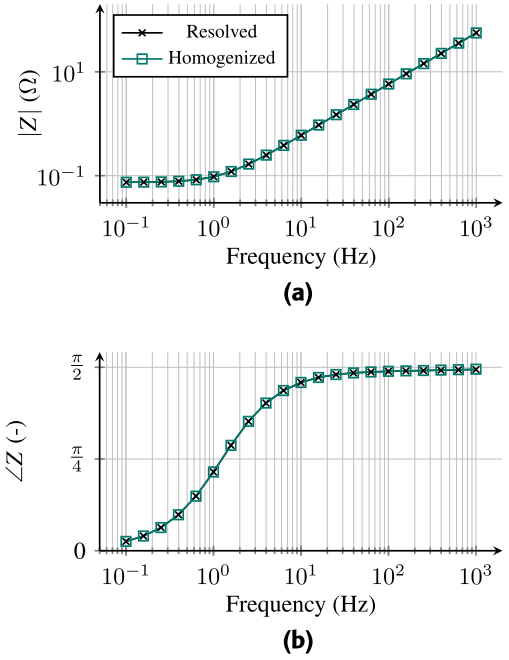

FIGURE 4. Comparison of the simulated impedance Z of the foil winding using the foil conductor model and the fully resolved model. (a) The amplitude of the impedance. (b) The angle of the impedance.

The implemented foil conductor model is first validated against a model where the individual turns are modeled as solid conductors and each foil and insulation layer is spatially discretized. The implementation of this resolved model is not further discussed here as it follows well established practices. The models are compared in the frequency domain in a Cartesian 2D setting, and a sufficiently fine mesh is used to keep the discretization error small. The foil conductor model is simulated with a mesh of 78 093 nodes and $N_p = 7$ voltage basis functions, whereas the mesh of the fully resolved model consists of 221 482 nodes. Figure 4 shows the simulated impedance Z of the foil winding as a function of frequency. An excellent agreement between the models is observed. The result demonstrates the validity of the foil conductor model which is generally accepted in the literature, for example, see [6], [8], [9], [10], and [11].

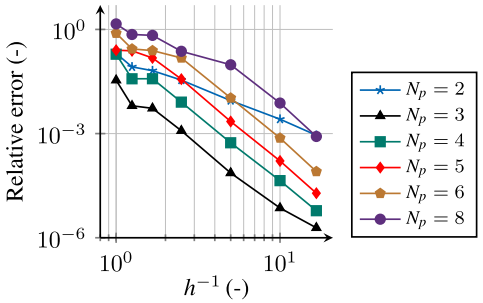

FIGURE 5. Relative error between the turn-by-turn conductance matrix definitions over the inverse of the mesh refinement parameter h for multiple values of N_p. The relative error is calculated using the Frobenius norm as $\|\mathbf{G} - \mathbf{G}_e\| \, \|\mathbf{G}_e\|^{-1}$.

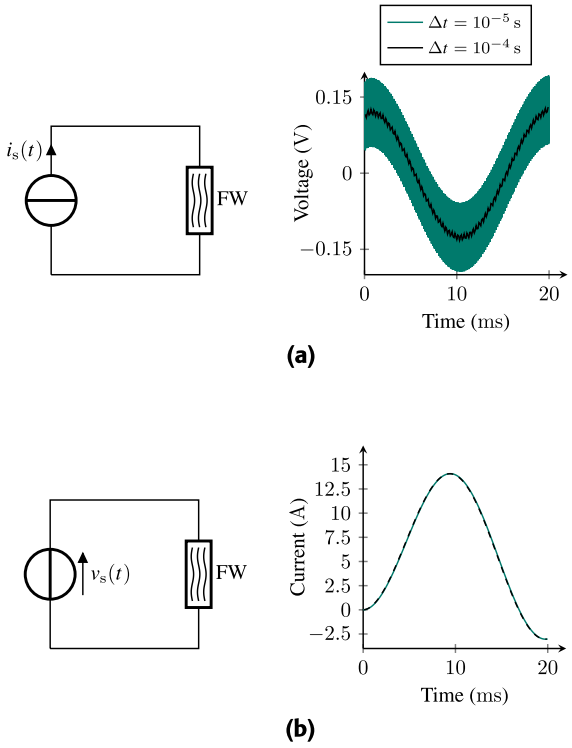

FIGURE 6. Current- and voltage-driven foil winding. (a) The perturbations that are added to the source current are amplified in the voltage over the foil winding. (b) No amplification of the perturbations of the source voltage occurs.

For the rest of the numerical tests, we will examine simulations on the time domain in a 2D axisymmetric geometry. Discretization in the time domain is done using the implicit Euler method with a constant time-step size. Let us examine the convergence of the turn-by-turn conductance matrix definitions (21) and (36). Figure 5 shows how the difference between the definitions decreases with increasing mesh refinement for multiple values of N_p. Convergence is observed in all situations. However, higher order polynomial approximations require increasingly fine meshes. We conclude that also the results of both foil conductor models converge to the same solution.

Next, the consequences of Proposition 1 for the simulation of the foil conductor model are demonstrated. The proposed new turn-by-turn conductance matrix (36) is used,

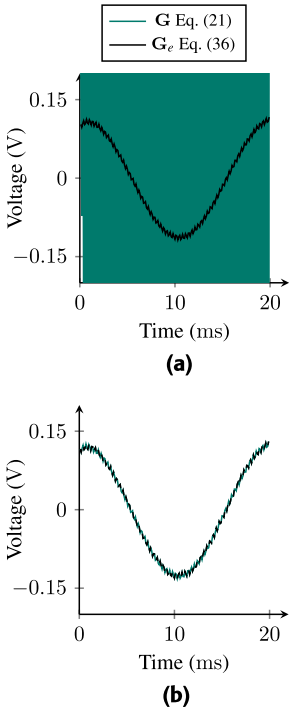

FIGURE 7. The voltage over the current driven foil winding with the different turn-by-turn conductance matrix definitions and mesh refinement. Different meshes with (a) 103 and (b) 1397 nodes.

and the modeling domain is spatially discretized with a mesh consisting of 1397 nodes. A voltage-driven foil winding is known to yield a system of DAEs with differentiation index 1, whereas the current-driven counterpart is an index-2 system. The sensitivity towards noise that these systems exhibit is examined by exciting them with a sinusoidal input which is perturbed with an additional sinusoid with small amplitude but high frequency. The magnitude of both the source voltage and current is given as $\sin(2\pi ft) + \epsilon \sin(2\pi f_\epsilon t)$.

Figure 6a shows the voltage over the current-fed foil winding. The perturbations of the source current are clearly amplified in the voltage output over the foil winding, and the amplification increases when the time-step size is reduced. The dependency of the amplification on the time-step size is a typical behavior of higher index DAEs, as larger time-steps are not able to resolve the (unwanted) high-frequency noise in the solution. When the model is excited with a voltage source, no perturbations are visible in the current through the foil winding, as can be seen in Fig. 6b. This corresponds to the expected behavior of an inductance-like element, which is less sensitive towards perturbations when excited with a voltage source than with a current source.

In the following, we compare the numerical behavior of the foil conductor model when using the two different turn-by-turn conductance matrices. The mismatch between the matrices $\|\mathbf{G}-\mathbf{G}_e\|$ is varied by refining the mesh. The earlier simulation setting is kept, and now only the current-driven model is examined. A time-step size of $\Delta t = 10^{-4}$ s is used.

Figure 7 shows the effect of reducing $\|\mathbf{G} - \mathbf{G}_e\|$ on the simulated voltage waveform. When $\|\mathbf{G} - \mathbf{G}_e\| \to 0$ through mesh refinement, the models coincide (numerically). This shows how the foil conductor model with the turn-by-turn conductance matrix $\mathbf{G}$ degenerates into an inductance-like element. With increasing $\|\mathbf{G} - \mathbf{G}_e\|$, the model becomes increasingly unstable and eventually diverges. A similar instability is not observed when using the proposed matrix $\mathbf{G}_e$.

V. CONCLUSION

This paper demonstrates that the classical definition of the foil conductor model is inconsistent in terms of circuit theory, i.e., the field model behaves in a circuit rather like a (singularly perturbed) resistor instead of an inductor. For coarse discretizations this may lead to instabilities in the time-stepping process. Therefore, we propose a simple modification to the turn-by-turn conductance matrix. The new formulation mitigates the problems with stability and leads provably to an inductance-like behavior. This is consistent with the behavior of eddy current fields excited with other conductor models such as the solid and stranded conductor ones. The introduced modification is always consistent, easy to implement in existing codes, and only marginally increases the computational cost.

APPENDIX I.
PROOF OF PROPOSITION 1

Define projector $\bar{\mathbf{Q}}$ onto $\ker(\bar{\mathbf{M}})$, and its complementary $\bar{\mathbf{P}} = \mathbf{I} - \bar{\mathbf{Q}}$. The projectors enable splitting (48a)

$$\bar{\mathbf{Q}}^\top \mathbf{K}_\nu \mathbf{a} = \bar{\mathbf{Q}}^\top \bar{\mathbf{x}} i \tag{49a}$$

$$\bar{\mathbf{M}} \frac{\mathrm{d}}{\mathrm{d}t}\mathbf{a} + \bar{\mathbf{P}}^\top \mathbf{K}_\nu \mathbf{a} = \bar{\mathbf{P}}^\top \bar{\mathbf{x}} i. \tag{49b}$$

The matrix $\bar{\mathbf{M}} + \bar{\mathbf{Q}}^\top \bar{\mathbf{Q}}$ is symmetric positive definite due to the definition of projector matrices and the symmetry of $\bar{\mathbf{M}}$. Multiplication of (49b) with $(\bar{\mathbf{M}} + \bar{\mathbf{Q}}^\top \bar{\mathbf{Q}})^{-1}$ and carrying out only algebraic manipulations yields

$$\begin{aligned}\bar{\mathbf{P}} \frac{\mathrm{d}}{\mathrm{d}t}\mathbf{a} &= \left(\bar{\mathbf{M}} + \bar{\mathbf{Q}}^\top \bar{\mathbf{Q}}\right)^{-1} \left(-\bar{\mathbf{P}}^\top \mathbf{K}_\nu \mathbf{a} + \bar{\mathbf{P}}^\top \bar{\mathbf{x}} i\right) \\ &= \mathbf{f}_{\mathbf{P}}(\mathbf{a}, i).\end{aligned} \tag{50}$$

One differentiation of (49a) with respect to time, and multiplication by $(\bar{\mathbf{Q}}^\top \mathbf{K}_\nu \bar{\mathbf{Q}} + \bar{\mathbf{P}}^\top \bar{\mathbf{P}})^{-1}$ gives

$$\begin{aligned}\bar{\mathbf{Q}} \frac{\mathrm{d}}{\mathrm{d}t}\mathbf{a} = &\left(\bar{\mathbf{Q}}^\top \mathbf{K}_\nu \bar{\mathbf{Q}} + \bar{\mathbf{P}}^\top \bar{\mathbf{P}}\right)^{-1} \\ &\cdot \left(-\bar{\mathbf{Q}}^\top \mathbf{K}_\nu \bar{\mathbf{P}} \frac{\mathrm{d}}{\mathrm{d}t}\mathbf{a} + \bar{\mathbf{Q}}^\top \bar{\mathbf{x}} \frac{\mathrm{d}}{\mathrm{d}t} i\right).\end{aligned} \tag{51}$$

Property (ii) of Assumption 1 ensures that the matrix $\bar{\mathbf{Q}}^\top \mathbf{K}_\nu \bar{\mathbf{Q}} + \bar{\mathbf{P}}^\top \bar{\mathbf{P}}$ is positive definite. Substituting $\frac{\mathrm{d}}{\mathrm{d}t}\mathbf{a}$ in (48b) allows solving the resulting equation with respect to the time derivative of the current

$$\begin{aligned}\frac{\mathrm{d}}{\mathrm{d}t} i = &\Bigg[- \bar{\mathbf{x}}^\top \left(\mathbf{I} - \bar{\mathbf{Q}} \left(\bar{\mathbf{Q}}^\top \mathbf{K}_\nu \bar{\mathbf{Q}} + \bar{\mathbf{P}}^\top \bar{\mathbf{P}}\right)^{-1} \bar{\mathbf{Q}}^\top \mathbf{K}_\nu \right) \\ &\cdot \mathbf{f}_{\mathbf{P}}(\mathbf{a}, i) - Ri + v \Bigg] L^{-1} \\ = &f_i(\mathbf{a}, i, v),\end{aligned} \tag{52}$$

where $\mathbf{I}$ is an identity matrix. The previous step required the inversion of $L = \bar{\mathbf{x}}^\top \bar{\mathbf{Q}} \left(\bar{\mathbf{Q}}^\top \mathbf{K}_\nu \bar{\mathbf{Q}} + \bar{\mathbf{P}}^\top \bar{\mathbf{P}}\right)^{-1} \bar{\mathbf{Q}}^\top \bar{\mathbf{x}}$, which is always possible when $L \neq 0$. This is guaranteed as it can be shown that $\bar{\mathbf{Q}}^\top \bar{\mathbf{x}}$ has full column rank. Consequently, L is positive (definite).

Substituting $\frac{\mathrm{d}}{\mathrm{d}t} i$ to (51) yields $\bar{\mathbf{Q}} \frac{\mathrm{d}}{\mathrm{d}t} \mathbf{a} = \mathbf{f}_{\mathbf{Q}}(\mathbf{a}, i, v)$. The explicit ODEs in Definition 2 have been obtained with only one time differentiation of (48), where the internal variables are $\mathbf{x} = \mathbf{a}$.

APPENDIX II.
PROOF OF PROPOSITION 2

Similarly as in the proof in Appendix I, we start by splitting (this time) the original discretization of the eddy current equation (28a) with the projectors $\mathbf{Q}_\sigma$ onto $\ker \mathbf{M}_\sigma$ and its complementary $\mathbf{P}_\sigma$. This leads to

$$\mathbf{M}_\sigma \frac{\mathrm{d}}{\mathrm{d}t} \mathbf{a} + \mathbf{P}_\sigma \mathbf{K}_\nu \mathbf{a} - \mathbf{P}_\sigma \mathbf{X}_\sigma \mathbf{u} = \mathbf{0} \tag{53a}$$

$$\mathbf{Q}_\sigma \mathbf{K}_\nu \mathbf{a} - \mathbf{Q}_\sigma \mathbf{X}_\sigma \mathbf{u} = \mathbf{0}. \tag{53b}$$

With (53a) one obtains

$$\mathbf{P}_\sigma \frac{\mathrm{d}}{\mathrm{d}t} \mathbf{a} = \left(\mathbf{M}_\sigma + \mathbf{Q}_\sigma^\top \mathbf{Q}_\sigma\right)^{-1} \left(-\mathbf{P}_\sigma \mathbf{K}_\nu \mathbf{a} + \mathbf{P}_\sigma \mathbf{X}_\sigma \mathbf{u}\right). \tag{54}$$

One time differentiation of (53b) and using the property that $\mathbf{Q}_\sigma \mathbf{X}_\sigma = 0$ due to $\mathbf{X}_\sigma$ being zero outside the conducting region, we have

$$\mathbf{Q}_\sigma \frac{\mathrm{d}}{\mathrm{d}t} \mathbf{a} = -\left(\mathbf{Q}_\sigma \mathbf{K}_\nu \mathbf{Q}_\sigma + \mathbf{P}_\sigma^\top \mathbf{P}_\sigma\right)^{-1} \mathbf{Q}_\sigma \mathbf{K}_\nu \cdot \left(\mathbf{M}_\sigma + \mathbf{Q}_\sigma^\top \mathbf{Q}_\sigma\right)^{-1} \mathbf{P}_\sigma \left(\mathbf{K}_\nu \mathbf{a} - \mathbf{X}_\sigma \mathbf{u}\right). \tag{55}$$

With these two equations we obtained an ODE for $\frac{\mathrm{d}}{\mathrm{d}t} \mathbf{a} = \mathbf{P}_\sigma \frac{\mathrm{d}}{\mathrm{d}t} \mathbf{a} + \mathbf{Q}_\sigma \frac{\mathrm{d}}{\mathrm{d}t} \mathbf{a}$ with at most one time differentiation of the original system. Inserting now (54) into the equation for $\mathbf{u}$, (28b) leads to

$$\mathbf{u} = \left(\mathbf{G} - \mathbf{X}_\sigma^\top \left(\mathbf{M}_\sigma + \mathbf{Q}_\sigma^\top \mathbf{Q}_\sigma\right)^{-1} \mathbf{X}_\sigma\right)^{-1} \cdot \left(-\mathbf{X}_\sigma^\top \left(\mathbf{M}_\sigma + \mathbf{Q}_\sigma^\top \mathbf{Q}_\sigma\right)^{-1} \mathbf{P}_\sigma \mathbf{K}_\nu \mathbf{a} + \mathbf{c} i\right). \tag{56}$$

Differentiating the latter expression once in time and using (54)-(55) gives

$$\frac{\mathrm{d}}{\mathrm{d}t} \mathbf{u} = (\mathbf{G} - \mathbf{X}_\sigma^\top (\mathbf{M}_\sigma + \mathbf{Q}_\sigma^\top \mathbf{Q}_\sigma)^{-1} \mathbf{X}_\sigma)^{-1} \mathbf{c} \frac{\mathrm{d}}{\mathrm{d}t} i + \mathbf{f}_{\mathbf{u}}(\mathbf{a}, \mathbf{u}), \tag{57}$$

which is an ODE-like expression for $\frac{\mathrm{d}}{\mathrm{d}t} \mathbf{u}$. Note that, in contrast to the formal definition of a resistance-like element, $\frac{\mathrm{d}}{\mathrm{d}t} \mathbf{u}$ depends on $\frac{\mathrm{d}}{\mathrm{d}t} i$. This, however, does not change the index results of [32] and therefore the element still has the same behavior as a resistance-like element within a circuit. Now that we have obtained expressions for the internal variables of the element $\frac{\mathrm{d}}{\mathrm{d}t} \mathbf{a}$ and $\frac{\mathrm{d}}{\mathrm{d}t} \mathbf{u}$, we look for the final relation between the current i and voltage v. This is recovered by differentiating (28c) once and inserting (57). Hereby, the voltage-to-current relation

$$\frac{\mathrm{d}}{\mathrm{d}t} v = \mathbf{c}^\top (\mathbf{G} - \mathbf{X}_\sigma^\top \mathbf{M}_\sigma^+ \mathbf{X}_\sigma)^{-1} \mathbf{c} \frac{\mathrm{d}}{\mathrm{d}t} i + \mathbf{c}^\top \mathbf{f}_{\mathbf{u}}(\mathbf{a}, \mathbf{u}), \tag{58}$$

which corresponds to a strongly resistance-like element if

$$\frac{\partial g_{\mathrm{R}}}{\partial \nu'} = (\mathbf{c}^\top (\mathbf{G} - \mathbf{X}_\sigma^\top \mathbf{M}_\sigma^+ \mathbf{X}_\sigma)^{-1} \mathbf{c})^{-1} \tag{59}$$

is positive definite. This is the case as long as $\mathbf{G} - \mathbf{X}_\sigma^\top \mathbf{M}_\sigma^+ \mathbf{X}_\sigma$ is nonsingular. In the last expressions we have replaced $\mathbf{X}_\sigma^\top (\mathbf{M}_\sigma + \mathbf{Q}_\sigma^\top \mathbf{Q}_\sigma)^{-1} \mathbf{X}_\sigma$ by $\mathbf{X}_\sigma^\top \mathbf{M}_\sigma^+ \mathbf{X}_\sigma$ with the Moore-Penrose pseudoinverse $\mathbf{M}_\sigma^+$. This is done to illustrate why $\mathbf{G}_e = \mathbf{X}_\sigma^\top \mathbf{M}_\sigma^+ \mathbf{X}_\sigma$ has been chosen and is possible because $\mathbf{Q}_\sigma \mathbf{X}_\sigma = 0$ due to construction and therefore both expressions are equivalent.

REFERENCES

[1] S. J. Salon, M. J. DeBortoli, and R. Palma, "Coupling of transient fields, circuits, and motion using finite element analysis," *J. Electromagn. Waves Appl.*, vol. 4, no. 11, pp. 1077–1106, Jan. 1990.
[2] G. Bedrosian, "A new method for coupling finite element field solutions with external circuits and kinematics," *IEEE Trans. Magn.*, vol. 29, no. 2, pp. 1664–1668, Mar. 1993.
[3] P. Dular, "Dual magnetodynamic finite element formulations with natural definitions of global quantities for electric circuit coupling," in *Scientific Computing in Electrical Engineering*. Warnemünde de, Germany: Springer, Aug. 2000, pp. 367–378. [Online]. Available: https://link.springer.com/book/10.1007/978-3-642-56470-3
[4] I. A. Tsukerman, "Finite element differential-algebraic systems for eddy current problems," *Numer. Algorithm.*, vol. 31, pp. 319–335, Dec. 2002.
[5] A. K. Das and B. G. Fernandes, "Accurate capacitance calculation of multi-layer foil windings in a medium/high-frequency high-power transformer," in *Proc. IEEE Energy Convers. Congr. Expo. (ECCE)*, Oct. 2020, pp. 5834–5841.
[6] M. Kazimierczuk and R. Wojda, "Foil winding resistance and power loss in individual layers of inductors," *Int. J. Electron. Telecommun.*, vol. 56, no. 3, pp. 237–246, Sep. 2010.
[7] M. Rios and G. Venkataramanan, "Design and construction of a foil winding permanent magnet machine," in *Proc. IEEE Energy Convers. Congr. Expo. (ECCE)*, Oct. 2020, pp. 2026–2033.
[8] D. Leuenberger and J. Biela, "Semi-numerical method for calculation of loss in foil windings exposed to an air-gap field," *IEEJ J. Ind. Appl.*, vol. 4, no. 4, pp. 301–309, 2015.
[9] H. De Gersem and K. Hameyer, "A finite element model for foil winding simulation," *IEEE Trans. Magn.*, vol. 37, no. 5, pp. 3427–3432, Sep. 2001.
[10] P. Dular and C. Geuzaine, "Spatially dependent global quantities associated with 2-D and 3-D magnetic vector potential formulations for foil winding modeling," *IEEE Trans. Magn.*, vol. 38, no. 2, pp. 633–636, Mar. 2002.
[11] C. A. Valdivieso, G. Meunier, B. Ramdane, J. Gyselinck, C. Guerin, and R. V. Sabariego, "Time-domain homogenization of foil windings in 2-D axisymmetric finite-element models," *IEEE Trans. Power Del.*, vol. 36, no. 3, pp. 1264–1269, Jun. 2021.
[12] M. Maciejewski, I. Cortes Garcia, S. Schöps, B. Auchmann, L. Bortot, M. Prioli, and A. P. Verweij, "Application of the waveform relaxation technique to the co-simulation of power converter controller and electrical circuit models," in *Proc. 22nd Int. Conf. Methods Models Autom. Robot. (MMAR)*, Aug. 2017, pp. 837–842.
[13] G. Benderskaya, M. Clemens, H. De Gersem, and T. Weiland, "Embedded Runge–Kutta methods for field-circuit coupled problems with switching elements," *IEEE Trans. Magn.*, vol. 41, no. 5, pp. 1612–1615, May 2005.
[14] K. Hameyer, S. Vandewalle, D. Lahaye, R. Mertens, and H. de Gersem, "Solution strategies for transient, field-circuit coupled systems," *IEEE Trans. Magn.*, vol. 36, no. 4, pp. 1531–1534, Jul. 2000. [Online]. Available: https://doi.org/10.1109/20.877729
[15] R. Escarela-Perez, E. Melgoza, and J. Alvarez-Ramirez, "Systematic coupling of multiple magnetic field systems and circuits using finite element and modified nodal analyses," *IEEE Trans. Magn.*, vol. 47, no. 1, pp. 207–213, Jan. 2011.

[16] S. Kanerva, "Data transfer methodology between a FEM program and a system simulator," in *Proc. 5th Int. Conf. Electr. Mach. Syst.*, Aug. 2001, pp. 1121–1124.
[17] S. Schops, H. De Gersem, and A. Bartel, "A cosimulation framework for multirate time integration of field/circuit coupled problems," *IEEE Trans. Magn.*, vol. 46, no. 8, pp. 3233–3236, Aug. 2010.
[18] A. Bartel, S. Baumanns, and S. Schöps, "Structural analysis of electrical circuits including magnetoquasistatic devices," *Appl. Numer. Math.*, vol. 61, no. 12, pp. 1257–1270, Dec. 2011.
[19] A. Bartel and M. Günther, "PDAEs in refined electrical network modeling," *SIAM Rev.*, vol. 60, no. 1, pp. 56–91, Jan. 2018.
[20] I. Cortes Garcia, H. De Gersem, and S. Schöps, "A structural analysis of field/circuit coupled problems based on a generalised circuit element," *Numer. Algorithms*, vol. 83, no. 1, pp. 373–394, Jan. 2020.
[21] S. Schöps, A. Bartel, H. De Gersem, and M. Günther, "DAE-index and convergence analysis of lumped electric circuits refined by 3-D MQS conductor models," in *Scientific Computing in Electrical Engineering SCEE 2008* (Mathematics in Industry), vol. 14, 2010, pp. 341–350.
[22] S. Schöps, H. De Gersem, and T. Weiland, "Winding functions in transient magnetoquasistatic field-circuit coupled simulations," *COMPEL, Int. J. Comput. Math. Electr. Electron. Eng.*, vol. 32, no. 6, pp. 2063–2083, Nov. 2013.
[23] A. Sihvola, *Electromagnetic Mixing Formulas and Applications*. Edison, NJ, USA: IET, 1999.
[24] A. A. Rodríguez and A. Valli, "Eddy current approximation of Maxwell equations," *Model., Simul. Appl.*, p. 347, 2010. [Online]. Available: https://link.springer.com/book/10.1007/978-88-470-1506-7
[25] P. Monk, *Finite Element Methods for Maxwell's Equations*. London, U.K.: Oxford Univ. Press, 2003.
[26] D. N. Dyck and J. P. Webb, "Solenoidal current flows for filamentary conductors," *IEEE Trans. Magn.*, vol. 40, no. 2, pp. 810–813, Mar. 2004.
[27] C.-W. Ho, A. E. Ruehli, and P. A. Brennan, "The modified nodal approach to network analysis," *IEEE Trans. Circuits Syst.*, vol. CS-22, no. 6, pp. 504–509, Jun. 1975.
[28] G. Hachtel, R. Brayton, and F. Gustavson, "The sparse tableau approach to network analysis and design," *IEEE Trans. Circuit Theory*, vol. CT-18, no. 1, pp. 101–113, Jan. 1971.
[29] E. Hairer, S. P. Nøsett, and G. Wanner, *Solving Ordinary Differential Equations II: Stiff and Differential-Algebraic Problems, Springer Series in Computational Mathematics*, 2nd ed. Cham, Switzerland: Springer, 2002.
[30] K. E. Brenan, S. L. Campbell, and L. R. Petzold, *Numerical Solution of Initial-Value Problems in Differential-Algebraic Equations*. Philadelphia, PA, USA: Society for Industrial and Applied Mathematics, 1995.
[31] D. Estévez Schwarz and C. Tischendorf, "Structural analysis of electric circuits and consequences for MNA," *Int. J. Circuit Theory Appl.*, vol. 28, no. 2, pp. 131–162, Mar. 2000.
[32] I. Cortes Garcia, S. Schöps, C. Strohm, and C. Tischendorf, "Generalized elements for a structural analysis of circuits," *Progress in Differential-Algebraic Equations II* (Differential-Algebraic Equations Forum). Cham, Switzerland: Springer, 2020.
[33] R. Albanese and G. Rubinacci, "Integral formulation for 3D eddy-current computation using edge elements," *IEE Proc. A Phys. Sci., Meas. Instrum., Manage. Educ., Rev.*, vol. 135, no. 7, pp. 457–462, 1988.
[34] J. Bundschuh, M. G. Ruppert, and Y. Späeck-Leigsnering, "Pyrit: A finite element based field simulation software written in Python," *COMPEL Int. J. Comput. Math. Electr. Electron. Eng.*, vol. 42, no. 5, pp. 1007–1018, Nov. 2023.

ELIAS PAAKKUNAINEN received the bachelor's and master's degrees in electrical engineering with specialization in electromechanics and power electronics from Tampere University, in 2019 and 2022, respectively. He is currently pursuing the Ph.D. degree with the Institute for Accelerator Science and Electromagnetic Fields, Technical University of Darmstadt. His research interests include multiscale modeling, homogenization techniques, and applied superconductivity.

JONAS BUNDSCHUH received the B.Sc. and M.Sc. degrees in electrical engineering and information technology from the Technical University of Darmstadt, in 2018 and 2020, respectively, where he is currently pursuing the Ph.D. degree in the topic of finite-element simulations of homogenized field models for foil windings. His research interests include homogenization techniques, finite element simulations, and scientific computing.

IDOIA CORTES GARCIA received the bachelor's degree in mathematics and the master's degree in modeling for science and engineering from the Autonomous University of Barcelona and the Ph.D. degree in electrical engineering from the Technical University of Darmstadt, in 2020. Since 2022, she has been an Assistant Professor with the Group of Dynamics and Control, Department of Mechanical Engineering, Eindhoven University of Technology. Her research interests include coupled multiphysical dynamical systems, differential algebraic equations, efficient time domain (co-)simulation methods, and hybrid modelling approaches.

HERBERT DE GERSEM (Member, IEEE) received the M.Sc. and Ph.D. degrees in electrical engineering from KU Leuven, Leuven, Belgium, in 1994 and 2001, respectively. From 2001 to 2006, he was with the Technical University of Darmstadt (TU Darmstadt), Darmstadt, Germany. Since 2001, he has been an Associate Professor with KU Leuven. Since 2014, he has been a Full Professor and the Head of the Institute for Accelerator Science and Electromagnetic Field (TEMF), TU Darmstadt. His research interests include finite-element electromagnetic field simulation for electrotechnical devices and particle accelerators and FDTD and FETD techniques for electromagnetic and ultrasonic wave propagation.

SEBASTIAN SCHÖPS (Member, IEEE) received the M.Sc. degree in business mathematics and the joint Ph.D. degree in mathematics and physics from Bergische Universität Wuppertal and Katholieke Universiteit Leuven. He was appointed as a Professor of Computational Electromagnetics with the Interdisciplinary Center of Computational Engineering, Technische Universität Darmstadt, in 2012. His current research interests include coupled multi-physical problems, bridging computer aided design and simulation, parallel algorithms for high performance computing, digital twins, uncertainty quantification, and machine learning.